Molecular Microbiology (2013) 90(4), 680–698 ■
doi:10.1111/mmi.12389
First published online 16 September 2013

Trapping and visualizing intermediate steps in the mismatch repair pathway *in vivo*

Justin S. Lenhart,[1†] Monica C. Pillon,[2†] Alba Guarné[2] and Lyle A. Simmons[1*]

[1]*Department of Molecular, Cellular, and Developmental Biology, University of Michigan, 830 North University Ave, Ann Arbor, MI 48109-1048, USA.*

[2]*Department of Biochemistry and Biomedical Sciences, McMaster University, 1280 Main Street West, Hamilton, Ontario L8S 4K1, Canada.*

Summary

During mismatch repair, MutS is responsible for mismatch detection and the recruitment of MutL to the mismatch through a mechanism that is unknown in most organisms. Here, we identified a discrete site on MutS that is occupied by MutL in *Bacillus subtilis*. The MutL binding site is composed of two adjacent phenylalanine residues located laterally in an exposed loop of MutS. Disruption of this site renders MutS defective in binding MutL *in vitro* and *in vivo,* while also eliminating mismatch repair. Analysis of MutS repair complexes *in vivo* shows that MutS mutants defective in interaction with MutL are 'trapped' in a repetitive loading response. Furthermore, these mutant MutS repair complexes persist on DNA away from the DNA polymerase, suggesting that MutS remains loaded on mismatch proximal DNA awaiting arrival of MutL. We also provide evidence that MutS and MutL interact independent of mismatch binding by MutS *in vivo* and *in vitro,* suggesting that MutL can transiently probe MutS to determine if MutS is mismatch bound. Together, these data provide insights into the mechanism that MutS employs to recruit MutL, and the consequences that ensue when MutL recruitment is blocked.

Introduction

Mismatch repair (MMR) is a highly conserved pathway responsible for identifying and correcting DNA polymerase errors, which substantially improves the overall fidelity of genome replication (Schofield and Hsieh, 2003; Kunkel and Erie, 2005; Iyer *et al*., 2006; Lenhart *et al*., 2012). Defects in bacterial MutS or MutL cause a large increase in mutation rate (Cox *et al*., 1972; Prudhomme *et al*., 1989; Ginetti *et al*., 1996; Davies *et al*., 2011; Cooper *et al*., 2012), while inactivation of the eukaryotic homologues, MutSα and MutLα, causes an increase in mutation rate and microsatellite instability (Fishel *et al*., 1994; Umar *et al*., 1994). In humans, disruption of MMR can lead to the development of sporadic cancers, as well as hereditary cancers such as Lynch and Turcot syndromes (Fishel *et al*., 1993; Hamilton *et al*., 1995; Nystrom-Lahti *et al*., 2002; Peltomaki, 2005). In prokaryotes, disruption of MMR can lead to an increased possibility of generating mutations that confer antibiotic resistance, and has been linked to antibiotic resistant strains of nosocomial human pathogens (Kluytmans *et al*., 1997; Lowy, 1998; Klein *et al*., 2007; Klevens *et al*., 2007).

In bacteria, the pathway and the mechanisms underlying MMR are best understood in the MutH and Dam containing bacterium *Escherichia coli*. In *E. coli*, MMR is initiated upon the recognition of single base mismatches or insertion/deletion loops (IDLs) by the mismatch binding protein MutS (for review Iyer *et al*., 2006; Larrea *et al*., 2010; Lenhart *et al*., 2012). While scanning for replication errors, MutS exists in an ADP bound state (Bjornson *et al*., 2000; Blackwell *et al*., 2001). Following mismatch recognition, a prominent model is that MutS exchanges ADP for ATP, converting MutS to a sliding clamp causing MutS to diffuse away from the mismatch along the DNA in search of MutL (Acharya *et al*., 2003; Winkler *et al*., 2011). After arrival, MutL then performs several tasks necessary to facilitate removal of the strand bearing the mismatch (Ban and Yang, 1998; Ban *et al*., 1999; Guarne *et al*., 2004).

The initial steps of MMR have been thoroughly studied and elucidated in the Gram-positive bacterium *Bacillus subtilis*, an organism lacking the Dam and MutH dependent pathway (for review Lenhart *et al*., 2012). Preceding mismatch detection, MutS is targeted to newly replicated DNA through interaction with the DNA replication processivity clamp DnaN (Simmons *et al*., 2008; Dupes *et al*., 2010; Klocko *et al*., 2011; Lenhart *et al*., 2012). DnaN, a critical component of the pathway, is required for 90% of MMR in *B. subtilis* (Lenhart *et al*., 2013). During Okazaki fragment maturation, DnaN accumulates behind the progressing replication forks forming a transient DnaN clamp

Accepted 29 August, 2013. *For correspondence. E-mail lasimm@umich.edu; Tel. (+1) 734 647 2016; Fax (+1) 734 647 0884. †These authors contributed equally.

zone that facilitates coupling between mismatch detection and concurrent DNA replication (Lenhart *et al*., 2013). Within this zone, MutS detects mismatches and initiates the downstream steps of repair, which includes MutL recruitment. The mechanism used by MutS to recruit MutL is unknown *in vivo* and *in vitro* for *B. subtilis*.

Even though MutS and MutL have been extensively characterized at the biochemical and genetic level, their binding interface and the mechanism used to recruit MutL is poorly understood in most organisms. In *E. coli*, an effort employing hydrogen/deuterium exchange mass spectrometry identified a MutL docking site on MutS composed of two adjacent glutamines (residues 211 and 212) found within the MutS connector domain (Mendillo *et al*., 2009). However, this site is not conserved in Gram-positive bacteria (Fig. S1), suggesting a separate uncharacterized interface that facilitates binding in other organisms. To our knowledge, no other sites have been identified in any bacterium lacking the Dam/MutH-dependent MMR, and the effect of MutS mutants defective for MutL interaction have not been tested on repair intermediates *in vivo* for any organism. Therefore, very little is known about MutL recruitment, yet this step represents the second step in one of the most important pathways for maintaining high fidelity replication in organisms from bacteria to humans.

Here we define the MutS•MutL interface in *B. subtilis*. We show that MutS binds the N-terminal domain of MutL via two adjacent phenylalanine residues, F319 and F320. Substitution of these phenylalanines to serine eliminates cross-linking of MutS to the N-terminal domain of MutL *in vitro* while also eliminating MMR *in vivo*. Importantly, these substitutions do not seem to affect other biochemical properties of MutS, including dimerization, ATPase activity, and mismatch binding. Furthermore, using single cell fluorescence microscopy, we show that MutS mutants defective in MutL interaction form repair centres that increase in both frequency within the cell population, as well as overall fluorescence intensity. These data provide *in vivo* evidence for *in vitro* models proposing that MutS loads repetitively at a mismatch. Our work also defines a regulatory role for MutL in limiting or preventing additional MutS dimers from loading at a mismatch. We show that repetitive loading of MutS is repressed following excision of the mismatch, which requires not only MutL recruitment but also endonuclease directed nicking of the DNA. We also provide evidence against the paradigm that MutL requires MutS bound to a mismatch to initiate interaction. We show that within living cells and with purified components, we can selectively cross-link MutS to MutL in the absence of a mismatch, suggesting a mechanism where MutL can transiently probe MutS to determine if MutS is indeed mismatch bound, and if so, license repair. Together, our data provide new insight into the MutL recruitment mechanism, the physiological consequences that result from MutS mutants unable to bind and recruit MutL, and we describe a model where MutL can transiently probe MutS before initiating the second step of MMR.

Results

The E. coli *MutL binding interface is not conserved in* B. subtilis

The MutS•MutL interface has previously been characterized in the Gram-negative bacterium *E. coli* (Mendillo *et al*., 2009). The interface is found within the connector domain of MutS, and centres around a double glutamine motif (Q211 and Q212) (Mendillo *et al*., 2009). Disruption of this site causes a loss of MMR *in vivo* and has been shown to eliminate interaction with MutL on a mismatched DNA substrate *in vitro* (Mendillo *et al*., 2009). Initially, we asked if the *E. coli* MutL binding motif was conserved in the Gram-positive bacterium *B. subtilis*; however, a sequence alignment revealed that the connector domain motif is not conserved, and the surrounding amino acid sequence is highly variable (Fig. S1A). Further examination of a *B. subtilis* MutS model shows that although the amino acid sequence in the connector domain is not conserved, the secondary and tertiary structure of the connector domain is conserved with that of *E. coli* MutS (Fig. S1B and C). Therefore, we mutated four residues, ^{205}VTII (*mutS Patch Ec*), which directly align with the *E. coli* ^{211}QQ motif, and occupy the corresponding location in a *B. subtilis* MutS model. Mutation of ^{205}VTII to ^{205}ASAA has no effect on MMR *in vivo*, conferring a mutation rate identical to the wild type control (2.47×10^{-9} mutations/generation [95% CI 0.95–3.82]) (Table 1, last row). With this result, we conclude that the MutL binding site on *B. subtilis* MutS is distinct from the site identified for *E. coli* MutS.

MutL binds several surface exposed peptides on MutS

We previously showed that a direct interaction between MutS and MutL can be detected in *B. subtilis* without a DNA substrate using a far Western blot (Klocko *et al*., 2010). To verify the direct MutS•MutL interaction, we performed a far Western blot to compare the binding of MutL to MutS and another known binding partner, the replication processivity clamp DnaN (Fig. 1A) (Simmons *et al*., 2008). We found that MutS retained MutL and DnaN on the nitrocellulose membrane during the binding reaction.

To identify candidate residues in MutS that may be important for MutL binding, we employed a peptide array library, which functions analogously to the far Western, using peptides in place of purified proteins. We screened a peptide array library composed of peptides representing the entire MutS primary structure. The MutS peptide library consisted of 10mer peptides offset by 3 residues, providing

Table 1. Mutation rate analysis of *mutS* patch variants.

Genotype	*mutS* variant	Number of cultures	Mutation rate (10-9 mutations/generation) ± [95% CI]	Relative mutation rate (% MMR activity)
Wild-type (PY79)	$mutS^{WT}$	24	3.30 [1.44–5.00]	1 (100%)
mutL::spec	$mutS^{WT}$	18	159.9 [152.5–167.2]	48.5 (0%)
mutS Patch 1	*E155S, R156S, L157A, E158S*	19	4.50 [2.23–6.64]	1.36 (99.2%)
mutS Patch 2	*E245S, E247S, E248S*	24	4.28 [2.10–6.34]	1.30 (99.4%)
mutS Patch 3A	*E306S, E307S, E310S*	25	4.19 [2.18–6.11]	1.27 (99.4%)
mutS Patch 3B	*F320S, E321S, R322S, E323S*	26	78.2 [72.2–84.2]	23.7 (52.1%)
mutS Patch 4	*E392S, E395S, E396S*	20	5.60 [2.59–8.40]	1.70 (98.5%)
mutS Patch 5	*E510S, E512S, E514S*	20	7.24 [4.45–9.94]	2.20 (97.5%)
mutS Patch 6A	*Q806A, L807A, F809A, F810A*	23	8.83 [6.03–11.58]	2.68 (96.5%)
mutS Patch 6B	*D811S, E812S, E814S*	20	3.03 [1.37–4.57]	0.92 (101%)
mutS Patch Ec	*V205A, T206S, I207A, I208A*	18	2.47 [0.95–3.82]	0.03 (101%)

All *mutS* variants were constructed using allelic replacement (see *Experimental procedures*), which maintains the *mutS* variant gene at its normal genetic locus and under the control of its native promoter, with the downstream *mutL* gene intact. Brackets enclose the lower bounds and upper bounds respectively of the 95% confidence limits. Percent MMR activity was determined using the following equation: [(R.M.R.null – R.M.R.strain)/(R.M.R.null – R.M.R.wild type)]•100; RMR = relative mutation rate. Relative mutation rate was obtained by dividing the mutation rate of each strain by that obtained for the wild type control.

threefold coverage of the entire sequence of MutS. We determined the association of MutL bearing a single C-terminal Myc tag with the MutS peptide array library in the presence of ADP and the non-hydrolysable ATP analogue adenosine 5′-(β,γ-imido) triphosphate (AMPPNP). We used ADP and AMPPNP to determine if the nucleotide bound state altered the putative MutL binding sites on MutS, because it has been previously shown that MutL undergoes substantial conformation changes during ATP binding and hydrolysis (Sacho *et al*., 2008).

We found that MutL•AMPPNP bound to 18 of 282 total peptides screened while MutL•ADP showed a nearly identical pattern and bound to 16 of the 18 peptides identified with MutL•AMPPNP (Fig. 1B, showing only surface exposed peptides**)**. Peptides 508 and 808 did not retain MutL–ADP binding (Fig. 1B). The data further shows that MutL–ADP bound at least one peptide in groups of overlapping peptides, suggesting that interaction within these regions occurred regardless of the nucleotide cofactor, and that overall, the nucleotide composition of MutL does not affect the specific MutS peptides bound. Further analysis of the amino acid composition of the MutS peptides bound by MutL–Myc revealed an enrichment of glutamic acid and phenylalanine residues, suggesting a preferred amino acid target on the MutS peptide array (Fig. S2).

To determine the location of each putative MutS binding peptides, we modelled *B. subtilis* MutS based on the *E. coli* and *Thermus aquaticus* structures (Lamers *et al*., 2000; Obmolova *et al*., 2000). In doing so, we found that most peptides (13 in the AMPPNP group and 11 in the ADP group) were surface exposed and located on the outer rim of the MutS dimer (Fig. 1B and C). Based on the location of the surface exposed peptides, we defined six unique regions (identified as patch 1–6) composed of single or multiple MutL–Myc bound peptides, which could facilitate an interaction between MutS and MutL (Fig. 1C). Since the peptides spanning residues 802–817 (patch 6) are absent from the crystal structures of *E. coli* and *T. aquaticus* MutS (Lamers *et al*., 2000; Obmolova *et al*., 2000), we were unable to include them in the model. Interestingly, patch 6, overlaps with the site known to bind DnaN, referred to as the DnaN clamp-binding motif (Fig. 1B, ^{806}QLSFF) (Dalrymple *et al*., 2001; Simmons *et al*., 2008). In *B. subtilis* mutation of this region does reduce MutL recruitment into foci although the mutant *mutS* still retains almost all MMR activity *in vivo* suggesting this region is not critical for binding MutL (Simmons *et al*., 2008).

Substitution of surface exposed residues within the putative MutL interaction sites on MutS causes defects in MMR

The peptide array analysis identified sites on MutS that could potentially mediate a direct interaction with MutL, thus we began by introducing three to four amino acid substitutions in residues both conserved and surface exposed within each ‘patch’ to determine the effect on repair (Table S1, for summary of substitutions). Each mutant *mutS* patch allele encoding a set of missense mutations was used to replace the wild type allele at the native *mutS* locus by allelic exchange as described (Lenhart *et al*., 2013). For each mutant allele, we determined the mutation rate by measuring the rate of spontaneous rifampin resistant colony formation as an indicator for mutagenesis and MMR dysfunction (Dupes *et al*., 2010; Klocko *et al*., 2011; Bolz *et al*., 2012; Lenhart *et al*., 2013 and *Experimental procedures*). Patch mutants 1, 2, 3A, 4, 5 and 6B conferred a statistically equivalent mutation rate to wild type *mutS*, showing no effect on the MMR pathway *in vivo* (Table 1). Patch mutant 6A, which contains the

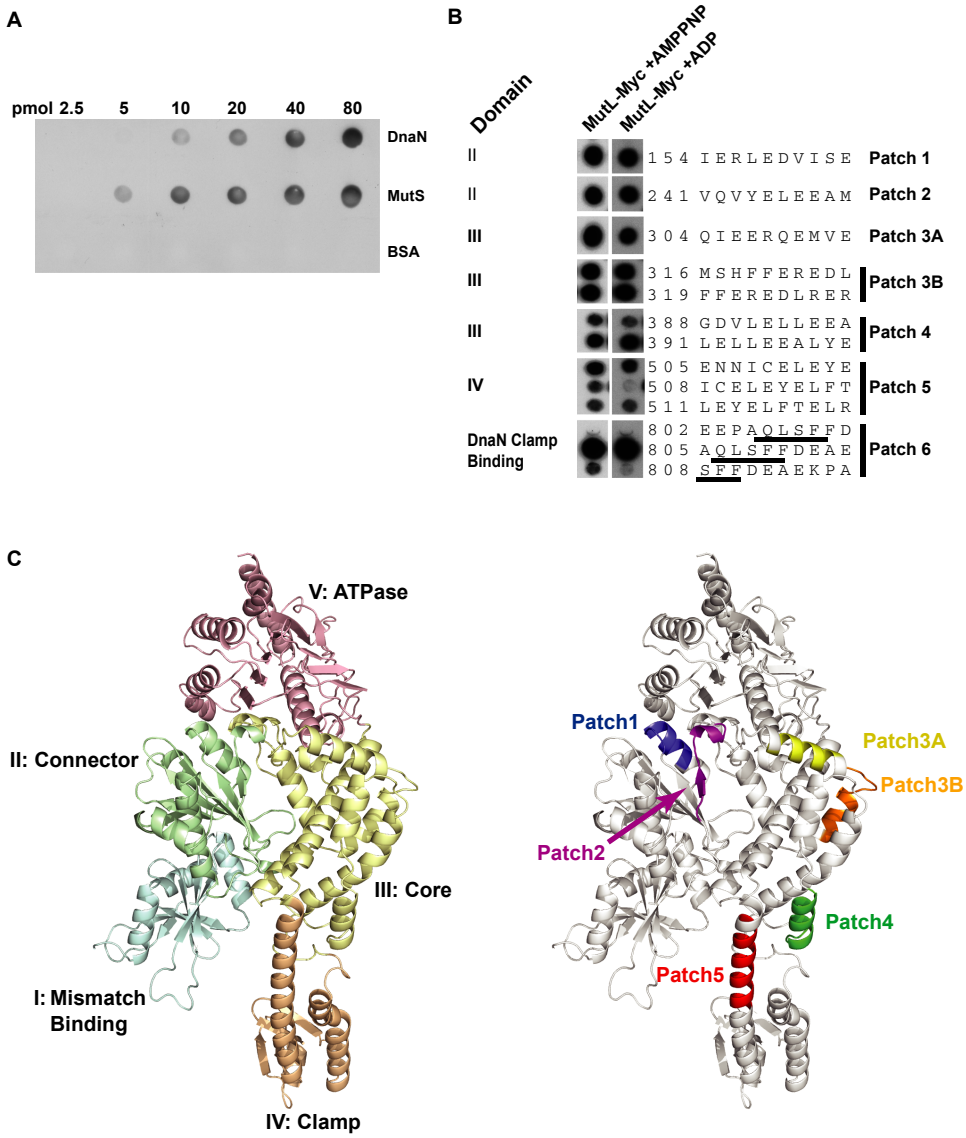

Fig. 1. *Bacillus subtilis* MutL binds surface exposed peptides in MutS.
A. A far Western blot using MutL to probe for interaction with purified MutS, DnaN, and BSA. Equal amounts of the indicated protein monomer was applied via a dot blot apparatus and probed with 0.4 μM purified MutL.
B. Screening of a MutS peptide array library with MutL–Myc. MutL–Myc was incubated with 0.5 mM of either ADP or AMPPNP during incubation with the peptide array. MutL–Myc bound peptides were detected with α-Myc antibodies. Indicated position of positive peptides on the array, as well as the amino acid sequence, is shown adjacent to the MutL–Myc bound peptides.
C. *B. subtilis* MutS was modelled using the SWISS-MODEL server (Arnold *et al.*, 2006). Both monomers of the model are shown as a ribbon diagram, with either the five functional domains of MutS (left panel) or the surface exposed peptides identified in the peptide array (right panel) colour-coded and labelled according to their representative patch definition.

DnaN clamp-binding motif, showed a slight but significant increase in mutation rate at 8.83×10^{-9} mutations/generation (Table 1) as we previously reported (Simmons *et al.*, 2008). Interestingly, we found that the four missense mutations introduced into patch 3B caused a significant increase in mutation rate (78.2×10^{-9} mutations/generation), resulting in this mutant retaining only 50% of MMR activity *in vivo*. With these data, we conclude that patch mutant 3B, which includes the *F320S*, *E321S*, *R322S*, and *E323S* missense mutations, causes a significant defect in the MMR pathway in *B. subtilis* (Table 1). Hereafter, we refer to the patch mutant 3B as MutS3B.

MutS3B is defective for interaction with MutL

The MutS•MutL interaction has been previously monitored using chemical cross-linking (Winkler *et al.*, 2011). The work by Winkler and co-workers demonstrated that

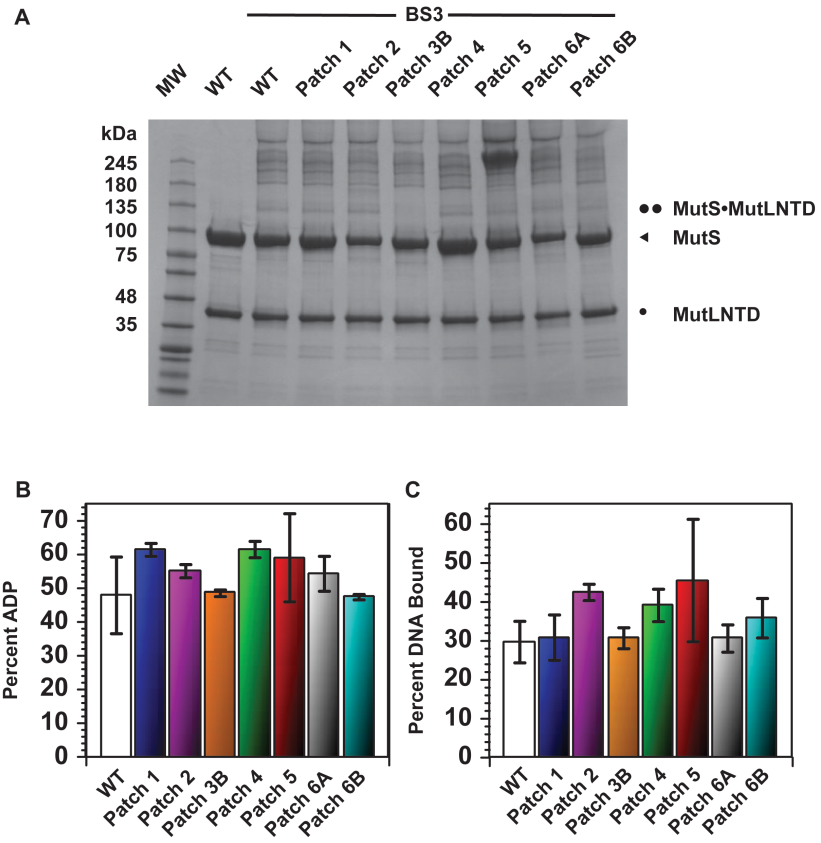

Fig. 2. Purified MutS3B fails to cross-link with the N-terminal domain of MutL.
(A) Cross-linking of MutS or MutS variants to the N-terminal domain of MutL with a 90 bp DNA substrate containing a centrally located G/T mismatch (Mis90). Mixtures of each protein, 10 mM ATP, and the G/T DNA substrate were incubated with the cross-linker BS3. Protein complexes were then resolved on a 4–15% gradient SDS polyacrylamide gel. The bands corresponding to the MutS and MutL–NTD monomers, as well as the MutS•MutL–NTD complex are labelled. All MutS variants show similar ATPase activity (B) and DNA binding to the G/T mismatched DNA substrate (C) to wild-type MutS. Bar diagrams present the average of three independent measurements and the error bars correspond to the standard errors of the mean (SEM = $\sigma/\sqrt{n}$, where σ is the standard deviation and n the sample size).

the MutS•MutL interaction only requires the N-terminal domain of MutL (MutL–NTD) and it is enhanced in the presence of ATP and a heteroduplex. Therefore, we purified N-terminal His_6 tagged variants of *B. subtilis* MutS and MutL–NTD and screened for interaction defects using this approach. Incubation of MutS and the chemical cross-linker bis(sulfosuccinimidyl)suberate (BS3) in the presence of ATP and a 90 base pair G/T mismatch DNA substrate (Mis90) resulted in the formation of several high molecular weight species. Conversely, incubation of MutL–NTD with BS3 predominantly yielded monomers, as expected due to the absence of the dimerization domain of the proteins. Incubation of MutS with MutL–NTD and BS3 in the presence of ATP and Mis90, yielded a new species that was not present when either protein was incubated with BS3 and corresponded to the molecular weight of the MutS•MutL–NTD complex (Fig. 2A). We excised this band, and using LC MS/MS, verified the presence of both MutS and MutL–NTD as the sole components of this band (data not shown). Interestingly, we do observe some interaction between MutS and MutL–NTD in the presence of a 90 bp DNA homoduplex in place of Mis90, showing that the MutS•MutL–NTD interaction is not strictly dependent on the presence of a mismatched substrate (Fig. S3).

We subsequently tested whether any of the MutS patch variants abrogated the interaction with MutL–NTD. We found that all MutS variants formed a MutS•MutL–NTD complex except for the MutS3B variant (F320S, E321S, R322S and E323S) (Fig. 2A). We note that the MutS5 variant (including the E510S, E512S and R514S mutations) showed a very prominent band of a molecular weight consistent with formation of a MutS tetramer. In fact, this prominent species was present in the cross-linking reaction of all MutS variants when MutL–NTD was not present (data not shown), but disappeared upon incubation with MutL–NTD. Since our goal was to probe for the formation of a MutS•MutL complex, and MutS5 retained the interaction with MutL–NTD, we did not characterize this variant further. The cross-linking defect of MutS3B agrees well with the mutation rate analysis showing that *patch 3B* lost 50% of MMR activity *in vivo* (Table 1). All 'patch' variants of MutS behave similar and have similar mismatch binding and ATPase activities compared with wild-type MutS (Fig. 2B and C), implying that the reduced MMR activity of the MutS3B variant is unlikely due to improper folding or attenuation of other critical biochemical activities. Furthermore, all of the MutS variants eluted from a gel filtration column similarly to the wild type protein (data not shown) and formed dimers in solution as measured by dynamic light scattering (Fig. S4). Collectively, we show that the

Table 2. Mutation rate analysis of missense mutations in and near *mutS3B*.

Genotype	Mutation rate (10-9 mutations/ generation) ± [95% CI]	Fold increase in mutation rate	% MMR activity
Wild-type (PY79)	3.30 [1.44–5.00]	1	100
mutL::spec	159.9 [152.5–167.2]	48.5	0
mutSS317A	2.62 [0.94–4.09]*	0.63	100.4
mutSH318S	2.36 [0.79–3.69]*	0.55	100.6
mutSF319S	105.1 [97.9–112.4]	31.9	35.0
mutSF320S	94.8 [87.3–102.4]	28.8	41.5
mutSE321S	4.02 [1.83–6.06]*	1.22	99.5
mutSR322S	2.46 [0.92–3.78]*	0.75	100.5
mutSE323S	148.7 [140.1–157.2]#	45.1	7.2
mutSF319SF320S	156.0 [148.9–163.1]#	47.3	2.5
mutSF319SF320S, *amyE::Pspac mutL*	134.0 [127.3–140.5]#	40.6	16.6

All *mutS* variants were constructed using allelic replacement (see *Experimental procedures*), which maintains the *mutS* variant gene at its normal genetic locus and under the control of its native promoter, with the downstream *mutL* gene intact. Brackets enclose the lower bounds and upper bounds respectively of the 95% confidence limits. Percent MMR activity was determined using the following equation: [(R.M.R.null − R.M.R.strain)/(R.M.R.null − R.M.R.wild type)]•100; RMR = relative mutation rate. Relative mutation rate was obtained by dividing the mutation rate of the strain by that of wild type. The symbols * and # indicates that the mutation rate is statistically equivalent to that of the wild type and MMR deficient strains respectively. For expression of *mutL*, 1 mM IPTG was added to the media during growth.

MMR defect associated with the MutS3B variant is due to the impaired interaction with MutL rather than loss of some other biochemical activity of MutS. Furthermore, we conclude that residues changed in the MutS3B (F320, E321, R322, and E323) variant are important for direct interaction between *B. subtilis* MutS and MutL–NTD.

Residues F319 and F320 define the MutL binding site on MutS

Since *mutS3B* contains four successive missense mutations, we replaced the native *mutS* gene in *B. subtilis* with alleles encoding each of the single missense mutations that comprise *mutS3B* using allelic exchange in order to further define the functional residues important for MutL interaction. We also included amino acids S317, H318, and F319 in this analysis due to their adjacent position in MutS relative to the peptide identified in the array and because each residue is predicted to be surface exposed. We found that mutation of F319S and F320S separately reduced MMR activity below 50% *in vivo* (Table 2). In addition, we found that *mutSE323S* had the most striking effect of all the single missense mutations on MMR as this allele supported only 7% of MMR activity *in vivo*. It should be noted that the effect observed in the *mutSE323S* mutant far exceeds that of the *mutS3B* mutant, which reduced MMR to 50% of wild type level. We suggest that the E321S and R322S substitutions may partially suppress the defect caused by E323S on its own. All other substitutions examined confer a mutation rate indistinguishable from wild type (Table 2). We did not pursue E323S for a role in MutL binding because this single mutant blocks MutS localization on its own and may have a folding defect. We describe the effects of this mutant later within this manuscript.

Because *mutSF319S* and *mutSF320S* showed significant and substantial defects in MMR, we combined these missense mutations to measure the effect on MMR *in vivo*. The resulting *mutSF319SF320S* allele showed a mutation rate (156×10^{-9} mutations/generation) indistinguishable from a strain lacking *mutL* (*mutL::spc*) function (Table 2). Immunoblot analysis verified that MutSF319SF320S, as well as MutS variants containing each individual mutation, accumulate to the same steady state levels as wild-type MutS *in vivo* (Fig. 3A). These results show that *mutSF319SF320S* phenocopies loss of *mutL* function in *B. subtilis* supporting the hypothesis that *mutSF319SF320S* is defective in MutL interaction. In addition we asked if overexpression of *mutL* could suppress the increased mutation rate caused by MutSF319SF320S. We expressed *mutL* using an IPTG inducible promoter from and ectopic locus and recovered only ~16% of MMR (Table 2, last row). This experiment further supports our conclusion that the MutSF319SF320S variant is substantially impaired for MutL interaction *in vivo*.

In order to determine if residues F319 and F320 of MutS define a MutL binding site, we purified MutSF319SF320S and tested its ability to interact with MutL–NTD using chemical cross-linking (Fig. 3B). Like MutS3B, MutSF319SF320S fails to cross-link with MutL–NTD, indicating that the mutation of the phenylalanine pair is sufficient to eliminate interaction between MutS and MutL *in vitro*. We also verified that these substitutions were wild type for other biochemical activities of MutS. MutSF319SF320S maintained wild type levels of ATPase activity, binding to mismatched DNA substrate, and dimer formation, by dynamic light scattering (Fig. 3C and D, and Fig. S4), suggesting that loss of *in vivo* MMR in the *mutSF319SF320S* background is attributed to loss of binding to MutL.

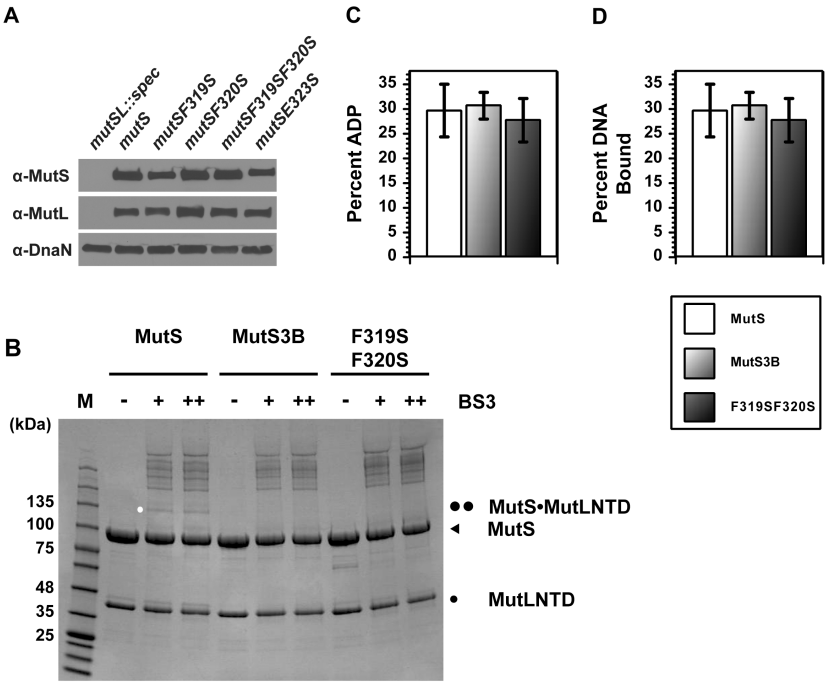

Fig. 3. A distinct di-phenylalanine binding site within and around MutS3B defines the MutL binding interface.
A. Immunoblot analysis indicated proteins from the soluble fraction of cell lysates. 50 μg of soluble fraction was probed for MutS, MutL and DnaN.
B. Complex formation of MutS, MutS3B, and MutSF319SF320S to the N-terminal domain of MutL was assayed on a 90 bp DNA substrate containing a centrally located G/T mismatch using cross-linking analysis. Reactions contained 10 μM MutS variants, 20 μM MutL–NTD, protein, 10 mM ATP, and 10 μM of the G/T DNA substrate were incubated with the hydrophilic cross-linker BS3 (+ = 0.8 mM and ++ = 1.6 mM respectively). The products were then separated on a 4–15% gradient SDS-PAGE. The bands corresponding to the MutS and MutL–NTD monomers, as well as the MutS•MutL–NTD complex are labelled. The biochemical activity of purified MutS, MutS3B, and MutSF319SF320S were tested for (C) ATPase activity and (D) DNA binding to the G/T DNA substrate. Bar diagrams present the average of three independent measurements and the error bars correspond to the SEM.

MutSF319SF320S defines a highly conserved MutL binding site on MutS in Gram-positive bacteria

We asked if the MutL binding site on MutS is conserved in other organisms. The MutS residues important for MutL binding, F319 and F320, model to the outer rim of MutS and reside in the loop connecting helices α4 and α5 of the core domain (Fig. 4A). Importantly, both residues appear solvent exposed, and available for interaction with MutL based on our structural model (Fig. 4A). In human MSH2 and the Gram-negative bacteria *E. coli* and *T. aquaticus* MutS, the site appears to be structurally conserved, despite the limited sequence conservation (Fig. 4B). Based on previous results (Mendillo *et al.*, 2009), this interface is not the sole binding interface for *E. coli* MutL, but may however function as a secondary site located on the opposite side of the MutS face. Importantly, helix α4 is part of the allosteric transmitter proposed to connect the ATP and DNA binding sites of MutS (Obmolova *et al.*, 2000), and hence, F319 and F320 pose an attractive mechanism to relay the nucleotide- and mismatch-bound state of MutS to MutL. Interestingly, we do find that the di-phenylalanine site is conserved in several eukaryotic proteins known to bind MutL homologue Mlh1 (Dherin *et al.*, 2009) including MutSβ (Fig. S5), as well as in anchoring interaction between mammalian Rev1 and Polκ (Iyer *et al.*, 2010; Wojtaszek *et al.*, 2012a,b) (see *Discussion*).

When we align MutS sequences from Gram-positive bacteria, many of which cause serious health concerns including *Staphylococcus aureus* and *Listeria monocytogenes*, we find that these residues are highly conserved in *mutS* homologues (Fig. 4C). In some Gram-positive bacteria, a few accepted substitutions are tolerated at these positions, such as the aromatic residue tyrosine or the hydrophobic residue isoleucine (Fig. 4C). Based on our results, we suggest that mutation of these conserved residues could eliminate MMR function in related pathogenic bacteria, increasing mutagenesis and altering antibiotic susceptibility and persistence within the host environment.

mutSF319SF320S *is defective for recruitment of MutL* in vivo

It has been previously shown that MutL–GFP forms foci in response to spontaneous or 2-aminopurine (2-AP) formed mismatches detected by MutS, providing an *in vivo* assay to monitor MutL recruitment in response to mismatch detection by MutS (Smith *et al.*, 2001; Lenhart *et al.*, 2013). A caveat with this assay is that the *mutL-gfp* allele is nearly defective for MMR as measured by mutation rate (Smith *et al.*, 2001); however, focus formation of MutL–GFP is dependent on *mutS*, providing a single cell assay for MutL–GFP recruitment in live cells (Smith *et al.*, 2001; Lenhart *et al.*, 2013). We asked if MutSF319SF320S was able to recruit MutL–GFP into foci in cells grown with 2-AP. In a background with the native *mutS* gene, we observed MutL–GFP repair centres in ~ 25% of cells (Fig. 5A). We found that cells with *mutSF319SF320S* or the Δ*mutS* allele did not support MutL–GFP focus formation, as MutL–GFP repair centres only formed in ~ 3% of the cell population in

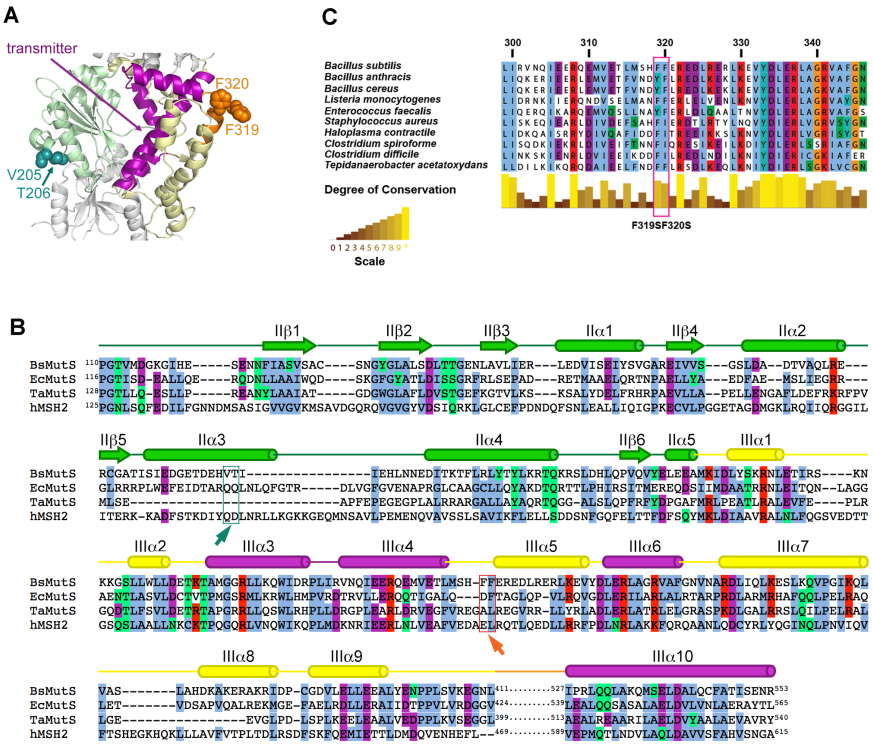

Fig. 4. The di-phenylalanine site is conserved in MutS homologues.
A. Ribbon diagram of the connector (light green) and core (light yellow) domains of MutS. The side-chains of the di-phenylalanine motif are shown in orange, those of the QQ motif are shown in teal (Mendillo *et al.*, 2009) and the structural elements of the transmitter proposed by Obmolova and co-workers belonging to the core domain are coloured in purple (Obmolova *et al.*, 2000).
B. Structure based sequence alignment of *B. subtilis* MutS and other MutS homologues for which the three-dimensional structure are known. Conserved hydrophobic (blue), polar (green), positive- (purple) and negative-charged (red) residues are highlighted. The secondary structure elements are colour-coded for domains II, domain III and transmitter as in A. The location of the QQ and FF motifs is indicated with teal and orange carets respectively.
C. Sequence alignment of MutS from Gram-positive bacteria shows conservation of F319 and F320.

both genetic backgrounds. Furthermore, we also found that MutSF319SF320S is defective for recruitment of MutL–GFP in response to mismatch detection *in vivo*, supporting the *in vitro* experiments showing that *mutSF319SF320S* is defective for interaction with MutL.

MutSF319SF320S forms large repair complexes in vivo*, supporting a model for persistent loading*

With a MutS variant defective in recruitment of MutL, we can now uncouple mismatch binding from functional repair and 'trap' repair intermediates that would normally be resolved during repair. To observe MMR intermediates, we fused *mutS* to a monomeric *gfpmut3* variant (*gfpmut3* referred to herein as *gfp*) since *gfpmut3* represents the most monomeric derivative of GFP, providing the least invasive method for observing protein localization in living bacterial cells (Landgraf *et al.*, 2012). We constructed a native locus *mutS-gfp* strain by allelic exchange in order to maintain expression of the downstream gene *mutL* under its native promoter (Fig. 5B). The *mutS-gfp* background maintained ~ 85% of MMR activity (mutation rate 2.56×10^{-8} [2.0–3.1]), providing a functional fusion to observe active repair in real time. Upon mismatch detection, MutS–GFP forms complexes in response to mismatches in order to orchestrate repair. The *mutS-gfp* strain forms repair centres in ~ 9% of cells within the population during exponential growth, and repair centre formation is stimulated to ~ 42% of cells by addition of 2-AP to the growth media (Fig. 5C, D, and E) (Simmons *et al.*, 2008; Dupes *et al.*, 2010; Klocko *et al.*, 2011; Lenhart *et al.*, 2013). Thus, using *B. subtilis*, we can bridge biochemical and genetic data to understand how disruption of MutL recruitment by MutS alters repair centre dynamics *in vivo*, providing important mechanistic insight into intermediate steps.

We subsequently fused *gfp* to *mutS3B*, *mutSF319S*, *mutSF320S*, *mutSF319SF320S*, and *mutSE323S* and found that all strains except for *mutSE323S-gfp* formed repair complexes *in vivo* (Fig. 5C). Interestingly, MutSE323S–GFP, which was defective for repair *in vivo*, was also completely defective for focus formation

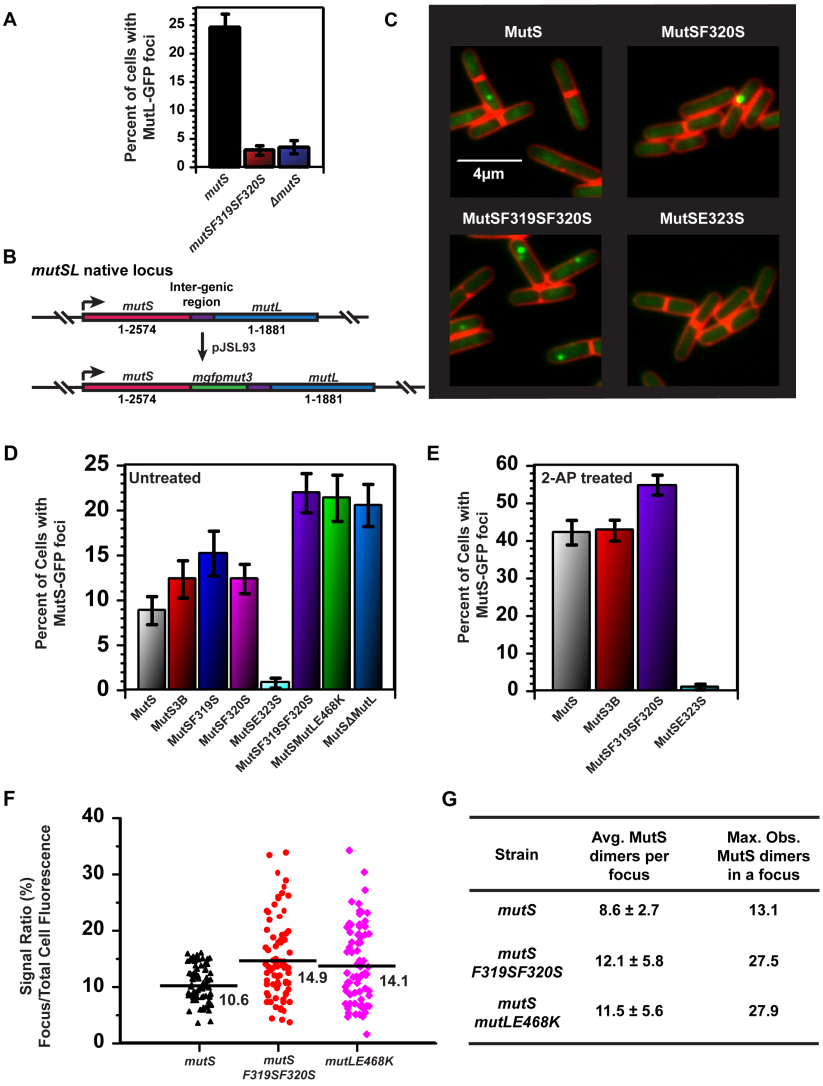

Fig. 5. MutS mutants defective for MutL interaction form persistent complexes *in vivo*.
A. Fluorescent single cell microscopy of MutL–GFP repair centres responding to mismatch formation in a *mutS*, *mutSF319SF320S* or *ΔmutS* background ($n = 1320$, 1559, and 988 cells scored). Cells were treated with 600 μg ml^{-1} of 2-AP and incubated for 1 h prior to imaging. 95% confidence intervals are shown.
B. Shown is a schematic for cloning an unmarked in frame fusion of *mutS* to *mutS-22-mgfpmut3* (*mutS-gfp*), while maintaining expression of the *mutL* gene downstream (*Experimental procedures*).
C. Representative micrographs of the indicated MutS–GFP fusion proteins. The cell membrane was imaged using the vital membrane stain TMA-DPH, which was pseudo-coloured red.
D. Shown is a bar graph of the percent of cells with each MutS–GFP fusion untreated during exponential growth ($n = 1276$, 957, 796, 1568, 1008, 1382, and 1148 respectively refers to the number of cells scored for each strain). Error bars represent 95% confidence intervals (CI). All groups are statistically significant with respect to MutS, including MutS Patch 3B ($P = 0.0038$) and MutSF320S ($P = 0.0013$). The strain with *ΔmutL* has a *mutS-mgfpmut2* fusion.
E. The percent of cells with the indicated MutS–GFP fusion following challenge with 2-AP ($n = 879$, 1212, 711, and 725 are the number of cells scored respectively) the error bars represent 95% CI.
F. Focus intensity was determined by normalizing total signal of the repair centres to the total cell fluorescence. A total of 75 MutS–GFP foci were analysed for each group. All foci examined were in cells statistically equivalent in regards to area, length, and average intensity of cellular fluorescence.
G. Using the number of MutS molecules per cell (Fig. S6) and the average MutS repair centre fluorescent intensity F), we were able to determine the average number of MutS dimers per repair centre ± standard deviation, as well as the highest observed number of MutS dimers within repair centres scored.

suggesting that although this protein accumulates *in vivo* (Fig. 3A), the E323S mutation appears to cause some defect other than blocking MutL interaction, since it failed to form a repair complex. The MutSE323S variant was not amenable to recombinant expression and purification and therefore we did not further pursue characterization of this variant (data not shown).

MutSF319S–GFP, MutSF320S–GFP, and MutSF319SF320S–GFP all formed foci in a higher percentage of untreated cells than the MutS–GFP control. We hypothesized that the increase in focus formation is a consequence of an increase in the duration of repair centre existence due to unproductive repair caused by a failure to properly signal for MutL. Another possibility is that there is an increase in mismatch detection, however, we ruled out this possibility by showing that a deletion of *mutL* downstream of *mutS-gfp* causes the same effect by increasing MutS–GFP repair centres *in vivo* (Fig. 5D). Furthermore, since the error rate of the replication process in the absence of functional MMR is one mispair every two rounds of replication the likelihood of closely spaced errors is extremely low (Bolz *et al*., 2012; Lenhart *et al*., 2013 and Table 1). Time-lapse imaging of repair centre formation and resolution would be preferred to support our hypothesis, but is not feasible due to long exposure times of the MutS–GFP fusions and rapid photobleaching dynamics (data not shown). MutSF319S–GFP, MutSF320S–GFP, and MutS3B–GFP formed repair complexes in a nearly indistinguishable percentage of cells (12–13% of the population) (Fig. 5D). The double mutant, MutSF319SF320S–GFP, shows an increase in the percentage of cells with MutS–GFP foci above our measurements for each of the single variants (Fig. 5D). Furthermore, 2-AP treatment elicited an increase in the percentage of cells with MutSF319SF320S–GFP, showing that this variant still binds mismatches and initiates repair, further supporting our *in vitro* results that mismatch binding is unaffected (Figs 5E and 3D). Ultimately, loss of MutL recruitment by MutS causes a corresponding increase in the percentage of cells with MutS repair complexes.

We also asked if MutS repair centre formation is not only affected by MutL recruitment, but also by the next step of repair – incision. To do so, we asked if MutS–GFP repair centres accumulate in cells where MutL endonuclease nicking is prevented using the *mutLE468K* allele (Pillon *et al*., 2010). Nicking by MutL is a required step for repair and we have previously shown that the E468K substitution eliminates MutL endonuclease activity *in vitro* and MMR activity *in vivo* (Pillon *et al*., 2010). Indeed, the percentage of cells with MutS–GFP foci increased in the *mutLE468K* background to levels observed in both the *mutSF319SF320S* and the *ΔmutL* backgrounds, indicating that if MutL-directed nicking is prevented, MutS–GFP foci persist when the next step of repair is blocked (Fig. 5D). With these data we argue that MutL recruitment is not sufficient to halt MutS loading *in vivo per se*, but that timely repair of the mismatch is required to prevent further loading.

We also found that a proportion of repair centres exhibited high fluorescence intensity in backgrounds defective for MutL recruitment and MutL endonuclease activity (Fig. 5C, F and G). We quantified percent focus intensity relative to whole cell fluorescence intensity. In doing so, we found that many repair centres associated with MutSF319SF320S had elevated focus intensities relative to a MutL recruitment proficient MutS–GFP strain (Fig. 5F). These data suggest that more MutS protomers are present in a focus for MutS mutants defective in MutL interaction or in strains where MutL function has been eliminated by blocking incision (*mutLE468K*) (Fig. 5F). We also analysed MutSF319SF320S foci in cells where *mutL* expression was induced and observed no difference in percent of cells with foci or focus intensity (data not shown).

We quantified the number of MutS dimers found within *B. subtilis* under the exact conditions used during live cell imaging, and found that in *B. subtilis* steady state levels of MutS are ~ 80 dimers per cell (100 nM) (Fig. S6). Using these data, we determined that the mean number of MutS dimers in a repair centre was ~ 8.5 (this corresponds to 17 GFP moieties) (Fig. 5G). Both the MutL recruitment and endonuclease-deficient backgrounds contained a higher mean number of MutS–GFP dimers per repair centre (12.1 and 11.5 respectively) (Fig. 5G). The increase in repetitively loaded MutS–GFP dimers is more pronounced in the broad distribution of individual intensity measurements of the repair centres, with as many as > 3-fold (~ 30 MutS–GFP dimers; ~ 35% of cellular MutS) more molecules in the highest intensity MutS complexes observed in repair deficient strains. These observations support a model where MutS can load iteratively at a mismatch, increasing the local concentration of MutS. We propose that iterative MutS loading aids in efficient MutL recruitment to the mismatch, providing *in vivo* support for *in vitro* observations (Acharya *et al*., 2003). We also find it interesting that we quantify 8.6 ± 2.7 MutS dimers per focus and in *S. cerevisiae* the number of Msh6 dimers per focus was determined to be 10.8 ± 4.4 (Hombauer *et al*., 2011). Therefore, the stoichiometry of MutS within a focus is remarkable similar between these two organisms.

mutSF319SF320S repair centres localize away from the replisome

During DNA replication, chromosomal DNA is replicated within an organized replisome (Lemon and Grossman, 1998; 2000; Berkmen and Grossman, 2006). Here, the replisome is defined as replication associated proteins that localize as discrete foci *in vivo*. Within *B. subtilis*, repli-

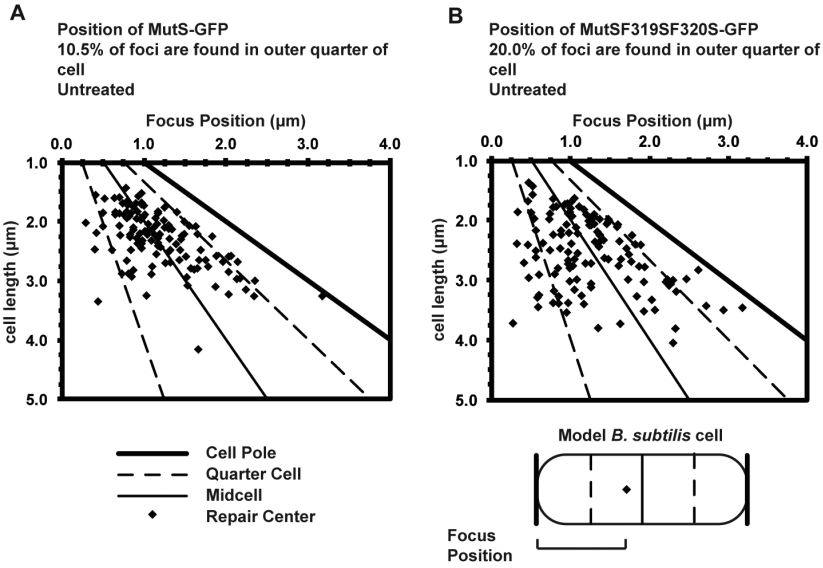

Fig. 6. MutSF319SF320S foci persist on DNA away from the replisome in the absence of MutL recruitment. The position of repair centres for (A) MutS–GFP and (B) MutSF319SF320S–GFP within each cell was plotted by the co-ordinates (cell length, distance to pole). Solid black line indicates midcell, whereas dashed lines indicates the quarter cell positions. The thick black line indicates the cell end. $n = 125$ (C) Table indicating colocalization values for MutS–GFP with DnaX–mCherry. The number of cells scored is indicated (n). P-values: * = 0.00052, ** =0.040, # = 0.0090, and difference between the 2-AP treatment groups = 0.105.

C

Colocalization of MutS-GFP foci with the Replisome (DnaX-mCherry)

Fusion	Addition of 2-AP	% colocalization (+/- 95% CI)	No. of cells analysed	
MutS-GFP	-	51.3% (7.8)	158	*
	+	35.0% (5.8)	260	#
MutSF319SF320S-GFP	-	38.2% (7.4)	165	**
	+	29.4 % (6.4)	197	

somes maintain a well-characterized subcellular position (Lemon and Grossman, 1998; 2000; Berkmen and Grossman, 2006). Once replication is initiated from the single origin of replication (*ori*), two sets of replication forks are often contained within a single replisome predominantly found at midcell (Lemon and Grossman, 1998; 2000; Berkmen and Grossman, 2006). Once replicated, the daughter chromosomes begin to translocate to the cell poles, taking mismatched DNA away from the centrally located replisome. We have previously shown that MutS foci colocalize to the replisome preceding mismatch detection and are released following mismatch binding (Lenhart *et al*., 2013). Therefore, we asked if localization of MutS repair complexes is altered when MutS is broken for MutL recruitment.

In order to test if the MutSF319SF320S repair centres persist at the site of mismatch identification, we monitored their position during DNA replication in minimal medium under slow growth conditions (~ 123 min doubling time). Slow growth maintains approximately half of the cell population with a single replisome focus (~ 52% of cells). We first determined the distance of the MutS and MutSF319SF320S repair centres relative to the cell poles (Fig. 6A). MutS–GFP repair centres maintain a mostly midcell position with 48.4% found within the middle 10% of the cell. Only 10.5% of these repair centres occupy a distal position within the outer quarters of the cell. Relative to the distribution of MutS–GFP, MutSF319SF320S–GFP position was more dispersed, as only 27.2% of repair centres were found within the middle 10% of the cell (Fig. 6B). About twofold more MutSF319SF320S repair centres (20%) were found in the distal quarter of the cell. These data support the hypothesis that upon identifying a mismatch at the replisome, the assembled MutS repair centre is maintained at the site of the mismatch for extended periods of time, causing migration away from the replisome as DNA synthesis continues, an effect more pronounced when MutL recruitment is blocked.

To further test this hypothesis, we examined colocalization between the MutS–GFP repair centres and replisomes during the same slow growth conditions described above. Colocalization between MutS–GFP and DnaX–mCherry (a component of the processivity clamp loader complex) was performed and scored as described (Lenhart *et al*., 2013). During exponential growth, MutS–GFP forms repair complexes that colocalize with the replisome in about 51% of cells. When we stimulate mismatch formation by adding 2-AP to the media, we found a decrease in colocalization to ~ 35% ($P = 0.00052$), consistent with previous results (Fig. 6C) (Lenhart *et al*., 2013). During exponential growth, MutSF319SF320S repair complexes colocalize with the replisome in 38% of the population; a significant decrease compared with MutS–GFP during exponential growth ($P = 0.0090$). Upon treatment with 2-AP, only 29% of repair

complexes colocalize with the replisome. With these results we conclude that when MutS–GFP is unable to recruit MutL to the site of a mismatch, repetitive loading of MutS–GFP at the mismatch will continue, resulting in a brighter and more persistent MutS–mismatch complex, which migrates away from the replisome as replication continues.

MutL cross-links with MutS independent of mismatch detection in vivo *and* in vitro

An outstanding problem in MMR is understanding how MutL senses when MutS is mismatch bound to initiate downstream steps of repair. Previously, we showed that the *mutSF30A* allele, supports formation of more MutL–GFP repair centres than are observed in the *ΔmutS* background (Lenhart *et al*., 2013). MutSF30A is a variant that is unable to distinguish mismatched DNA from complementary DNA (Lenhart *et al*., 2013). This observation is interesting because it suggests that MutS can interact with MutL, in the absence of mismatch binding *in vivo*, even though the interaction is reduced (Lenhart *et al*., 2013). Here, we directly test the hypothesis that MutL can transiently probe MutS for the appropriate conformational change to initiate MMR. To test this hypothesis, we used immunoprecipitation (IP) targeting MutS to co-IP any proteins associated with MutS *in vivo*. Since the MutS•MutL interaction is transient in nature, we employed the use of the thiol-cleavable, membrane permeable cross-linker Dithiobis[succinimidyl propionate] (DSP) to cross-link MutS•MutL complexes formed in growing cells (Fig. 7).

The IP was accomplished under normal growth conditions in the absence of 2-AP to test for association in the absence of active MMR. Using this procedure, we were able to IP ~ 10.0% of the intracellular MutS. Importantly, we were able to capture the MutS•MutL interaction in the wild type strain, yet failed to IP MutL in the *ΔmutS* strain, validating the requirement of MutS for successful co-IP of MutL. We were able to detect a MutL band (0.02% of input) in the IP lane from the wild type strain. The low amount of MutL recovered in the wild type strain is likely because we are precipitating only 10.0% of intracellular MutS, as well as we expect only 9% of cells to have ongoing MMR as determined by the assembly of active MutS–GFP repair centres. In agreement with our *in vitro* data and the MutL–GFP microscopy (Table 2 and Fig. 5A), we recovered low amounts of MutL in the IP lane from the *mutSF319SF320S* lysate (< 0.001% of the input), confirming that MutSF319SF320S is compromised for interaction with MutL *in vivo* (Fig. 7). In Fig. 7, we also present error measurement from three independent IP experiments. In the other experiments performed we did not recover any detectable amount of MutL in the MutSF319SF320S lysate

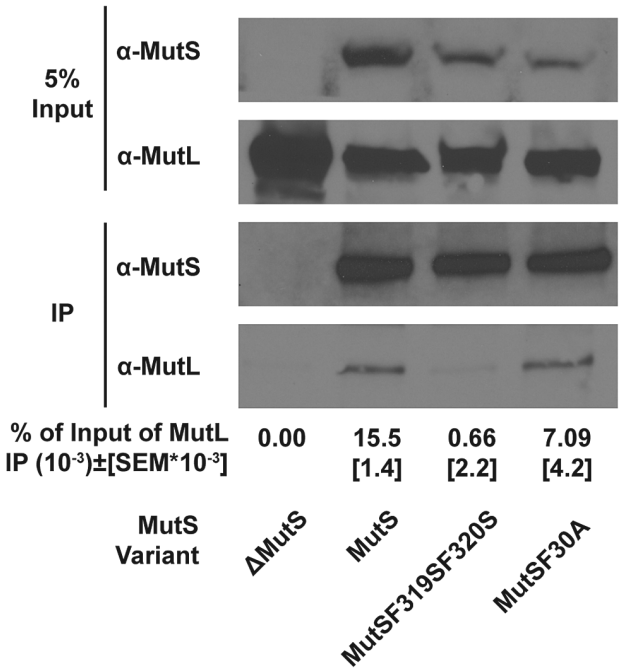

Fig. 7. MutS cross-links with MutL in the absence of mismatch detection *in vivo*. Co-immunoprecipitation of MutS and MutL in the indicated backgrounds with affinity purified polyclonal antibodies against MutS. MutS and MutL levels were probed for using antiserum directed against MutS or MutL. Band intensity was determined using ImageJ quantification software (See *Experimental procedures*). Relative IP MutL levels reflect absolute band intensity per lane normalized to the wild type MutS lane. The error (SEM) were calculated from 3 independent experiments.

further supporting our conclusion that this mutant does not interact with MutL (data not shown).

We then tested whether mismatch detection was necessary to facilitate MutS•MutL interaction *in vivo*, speculating that MutL may frequently probe MutS for the appropriate protein conformation, signalled by mismatch detection. To test this, we IPed MutSF30A: a MutS variant capable of DNA binding, yet incapable of discriminating mismatched DNA from complementary DNA (Lenhart *et al*., 2013). When MutSF30A was immunoprecipitated, we found that we successfully captured MutL (~ 0.007% of input). This result shows that the MutS•MutL interaction may dynamically occur independent from mismatch identification *in vivo*, suggesting that MutL is capable of transiently 'checking' to determine if MutS is mismatch bound before licensing downstream repair events. Similar observations have been seen in *S. cerevisiae in vitro* showing that MutSα interaction with MutLα is not entirely mispair dependent (Kijas *et al*., 2003).

Discussion

Here, we have identified a conserved MutL binding site on MutS in the Gram-positive bacterium *B. subtilis*. Using

peptide array mapping, extensive mutagenesis, single-cell fluorescence microscopy and *in vitro* cross-linking studies, we have identified residues found within the core domain, important for MMR *in vivo* and interaction with MutL–NTD *in vitro*. This site was further refined to a discrete MutL docking site composed of adjacent phenylalanine residues F319 and F320. Substitution of both phenylalanines to serine completely eliminates MMR *in vivo* and is defective for cross-linking to MutL–NTD *in vitro*. We also show that purified MutSF319SF320S is similar to wild type MutS for dimerization, ATPase activity, and binding to mismatched DNA substrates. We can therefore attribute the loss of MMR *in vivo* to a failure in MutL binding and recruitment. To our knowledge this effort defines the first MutL binding site on MutS in a bacterial organism lacking a methylation-directed MMR pathway.

Importantly, the di-phenylalanine motif that we identified in *B. subtilis* MutS to mediate interaction with MutL appears to be conserved and is part of a larger S[X]FF motif known to mediate MutL interaction with eukaryotic proteins. In *S. cerevisiae*, the S[X]FF motif was shown to be important for interaction between eukaryotic MutL homologue (Mlh1) and several Mlh1 bindings partners including Exo 1, BLM and Sgs1 proteins (Dherin *et al*., 2009). Furthermore, a S[X]FF motif was also shown to mediate interaction between MutSβ (Msh2–Msh3) and MutLβ (Mlh1–Pms2), for the human proteins (Iyer *et al*., 2010). In addition, a di-phenylalanine motif has been shown to be critical for interaction between mammalian translesion polymerases Rev1 and pol κ (Wojtaszek *et al*., 2012a,b). Our results in consideration with those above, show that adjacent phenylalanine residues play important roles in mediating protein interactions in a wide variety of organisms.

Previous analysis of the *E. coli* MutS•MutL interaction identified residues in the mismatch recognition and connector domains involved in this interaction (Mendillo *et al*., 2009; Winkler *et al*., 2011). However, the connector domain of *E. coli* MutS on its own only weakly interacts with MutL, suggesting that additional surfaces on MutS may be involved in this interaction. While the mismatch recognition and connector domains are in close proximity to the core domain, the residues identified previously in *E. coli* MutS (Q211 and Q212) and patch 3B (F319 and F320) reside in opposite faces of the monomer and are separated by the allosteric transmitter that connects the mismatch- and ATP-binding domains (Fig. 8). It is conceivable that the different techniques used in our study and that by Mendillo and co-workers may have revealed distinct anchoring points of the MutS•MutL interface. If true, the MutS•MutL complex could adopt two distinct architectures. MutL could interact with both protomers of the MutS dimer to form a productive complex (arrow ii in Fig. 8), thereby implying a mechanism to 'check' MutS for mismatch binding through contacts with the mismatch-binding domain that would support the distance restraints reported by Winkler and co-workers (Winkler *et al*., 2011).

Alternatively, MutL could interact with a single protomer of the MutS dimer (arrow i in Fig. 8). This model poses an attractive mechanism to sense the mismatch and nucleotide binding states of MutS. The mismatch- and the nucleotide-binding domains of MutS are connected by a transmitter helix that runs along the outer rim of the MutS protomer (Fig. 8) (Obmolova *et al*., 2000). Therefore, if MutL binds this face of MutS, the transmitter helix is probably a central feature of the interaction interface. This model also supports the established idea that only one of the MutS protomers mediates the interaction with MutL (Prolla *et al*., 1994; Habraken *et al*., 1997; Mendillo *et al*., 2009). Interestingly, mutation of patch 3A, which is part of the MutS transmitter, does not affect MMR *in vivo* (Table 1 and Fig. 1). However, the MutS3A variant could not be overexpressed recombinantly in *E. coli*, implying a stability defect that could result from mutation of the transmitter. This, in turn, implies that MutL senses a different region of the transmitter, potentially α-helix 10 located in the C-terminus of the core domain (Figs 4 and 8).

Upon identifying the binding interface, we extended our study to investigate the dynamic nature of MutS repair complexes *in vivo*. We present data showing that disruption of MutL recruitment causes repetitive MutS loading in response to mismatch formation. Since MutL recruitment is blocked we interpret this to mean that a MutS intermediate is 'trapped' because the downstream step is prevented and we find that MutS foci persist with the number of MutS dimers per focus increased. These results support a model for repetitive loading by MutS in response to mismatch formation. Furthermore, even upon successful recruitment of MutL to a mismatch, we show that loss of function due to disruption of the endonuclease active site phenocopies a *ΔmutL* allele, supporting the hypothesis that not only does MutS loading occur independent from MutL recruitment, but that endonuclease directed nicking, and presumably excision of the mismatch, is a critical feature to disassemble MutS complexes. As more dimers of MutS load onto the mismatch proximal DNA, more MutS is available to recruit MutL. In support of this hypothesis, real-time *in vitro* imaging of MutSα and MutLα on DNA curtains revealed that the interaction requires a mismatch, yet interaction between MutSα and MutLα may occur after MutSα formed the ATP hydrolysis-dependent sliding clamp (Gorman *et al*., 2012). Therefore, even mismatch-dissociated MutSα dimers can still facilitate a MutLα interaction, in essence amplifying a signal for MutL recruitment and for the advancement of repair. Our experiments represent *in vivo* data supporting repetitive loading of MutS at a mismatch, supporting previous *in vitro* experiments showing repetitive loading using circular mismatch containing substrates (Gradia *et al*., 1999; Acharya *et al*., 2003). In addi-

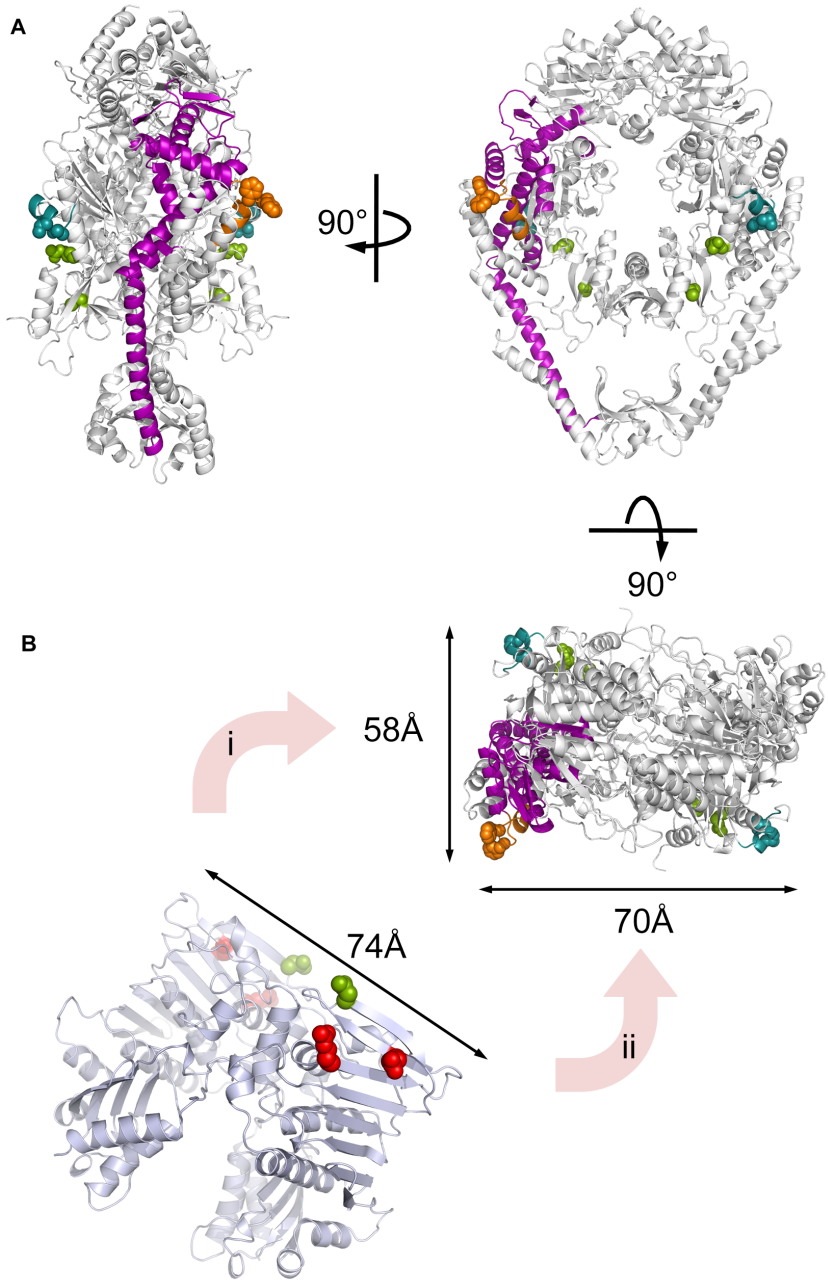

Fig. 8. Potential interfaces of the MutS•MutL complex.
A. Orthogonal views of the *B. subtilis* MutS dimer shown as a ribbon diagram with the residues deemed important for the interaction with MutL shown in orange (FF motif, this work), teal (QQ motif, Mendillo *et al.*, 2009) or green (distance constraints identified by cross-linking, Winkler *et al.*, 2011). The transmitter region of MutS is highlighted in purple.
B. Ribbon diagram of the *E. coli* MutL–NTD dimer shown as a ribbon diagram with the residues identified in cross-linking studies shown in green (Winkler *et al.*, 2011) and additional residues deemed important for the interaction with MutS shown in red (Plotz *et al.*, 2006). Dimensions of the MutS and MutL dimer surfaces are indicated in angstroms (Å) and the two potential surfaces of MutS that MutL could recognize are indicated with pink arrows and labelled i and ii respectively.

tion to providing evidence for repetitive loading *in vivo*, we also provide evidence that mismatch excision is an important step in disassembling MutS repair complexes.

After excision of the mismatch, MutS loading is halted and the already bound MutS dimers will dissociate from the DNA in a timely manner, leading to disassembly of the repair centre. *In vitro*, single molecule imaging reveals that after lesion recognition, the newly formed MutSα sliding clamp will remain on DNA with a lifetime of $t_{1/2} \geq 198 \pm 23.4$ s (Gorman *et al.*, 2012). If loading is restricted to nascent DNA, then defective repair centres should persist on DNA flanking mismatches for up to 10 min after initial mismatch recognition. Furthermore, as DNA replication continues, newly replicated DNA moves farther away from the replisome, taking newly formed mismatches with it. In support of the hypothesis that MutS repair centres defective for MutL recruitment persist longer on DNA surrounding the mismatch, the distribution of these MutS centres are located farther away from the replisome than repair centres engaging in active repair. Moreover, in exponentially growing cells, less repair centres colocalize with predominantly midcell replication centres. These two observations support the hypothesis that unproductive MutS repair centres persist on mismatch proximal DNA.

In *B. subtilis*, a model is emerging for the early steps of MMR *in vivo*. We propose that MutS is positioned at the replisome preceding mismatch detection by a DnaN clamp zone that results from Okazaki fragment maturation (Fig. S7A) (Lenhart *et al.*, 2013). MutS binds free DnaN clamps via a DnaN-binding motif (^{806}QLSFF) found in the unstructured C-terminal clamp-binding domain. MutS is able to find ~ 90% of mismatches through a DnaN coupled mechanism. Once MutS detects a mismatch, we propose that MutS (Fig. S7B) loads repetitively at the mismatch, producing numerous DNA-bound MutS dimers (Fig. S7C). We propose that repetitive MutS loading facilitates efficient MutL recruitment by increasing the local concentration of DNA bound MutS dimers surrounding the mismatch. MutS diffusing away from a mismatch with MutL may also help MutL identify strand discontinuities necessary to direct incision to the nascent strand (Fig. S7D). Finally, the data presented here support the model that MutL-incision is necessary for disassembly of MutS complexes suggesting that mismatch excision is important for preventing further MutS loading.

Overall, this work describes the interaction between the core domain of MutS and MutL both *in vitro* and *in vivo*, and the implications of this interaction for the recruitment and activation of MutL at MutS repair centres, providing insight into the intermediate steps of MMR in live cells.

Experimental procedures

Bacteriological methods

Bacillus subtilis strains were grown according to established procedures (Dupes *et al.*, 2010). Briefly, strains were grown in Luria–Bertani (LB) medium or defined $S7_{50}$ minimal medium. Unless otherwise stated antibiotics were used when appropriate with the following concentrations: 100 μg ml^{-1} spectinomycin (*spc*), 5 μg ml^{-1} chloramphenicol (*cam*), 5 μg ml^{-1} tetracycline (*tet*), 0.5 μg ml^{-1} erythromycin and 12.5 μg ml^{-1} lincomycin (*mls*), 5 μg ml^{-1} kanamycin (*kan*), 150 μg ml^{-1} rifampin (*rif*).

Peptide array analysis

The MutS peptide array was synthesized at the Massachusetts Institute of Technology Biopolymers laboratory, (Cambridge, MA). The synthesized MutS peptides provided 1× coverage spanned the entire amino acid sequence of MutS by overlapping 10 mer peptides offset by 3 residues. The final array consisted of 282 spotted peptides. The peptide array was activated by wetting with 100% ethanol, followed by 3 successive washes in Tris-buffered saline + Tween 20 (TBS-T) (50 mM Tris-Cl pH 7.5, 150 mM NaCl and 0.05% Tween 20) (pH 7.6) for 5 min to remove excess ethanol. The array was then blocked overnight in TBS-T and 10% milk solids at 4°C. The following day, the array was washed in TBS-T, and then incubated in 56 nM MutL-myc in protein incubating solution (40 mM HEPES-KOH pH 7.6, 23 mM KCl, 1 mM $MgSO_4$, 1 mM DTT, 0.5 mg ml^{-1} BSA, 2% glycerol, and 0.5 mM of either AMPPNP or ADP) for 15 h at 4°C with gentle rocking. The next day, the array was washed for 30 min total with 3 washes each of the following buffers in order: TBS-T, TBS-T with 500 mM NaCl, TBS-T + 0.5% Triton X-100, and TBS-T. The array was then incubated with 1:5000 α-myc antibody in TBS-T + 5% milk for 1 h at room temperature. The wash series was repeated, followed by incubation with 1:2000 anti-mouse in TBST + 5% milk for 1 h at room temperature. After antibody incubation, one more wash series was performed and the array was exposed using Pierce SuperSignal. Exposure time-course of 2 min, 5 min, and overnight were obtained to identify bound peptides.

False-positive peptides were removed by comparing with a negative control (no myc-tagged protein exposure). Finally, peptides that were surface exposed based on a structure-guided sequence alignment of MutS homologues were deemed putative MutL binding peptides.

Strains and plasmid

All *B. subtilis* strains used are derivatives of PY79 and are described in supplemental Table S2. Plasmids created for use in this study are as follow:

Bacillus subtilis mutS and *mutL* expressing plasmids MutS (pAG 8483; residues 1–858) was amplified from *B. subtilis* strain 168 genomic DNA and ligated into pET-15b (Novagen) using restriction sites NdeI and BamHI. MutS variants Patch 1 (pAG 8561; E155S, R156S, L157A, E158S), Patch 2 (pAG 8674; E245S, E247S, E248S), Patch 3B (pAG 8635; F320S, E321S, R322S, E323S), Patch 4 (pAG 8634; E392S, E395S, E396S), Patch 5 (pAG 8616; E510S, E512S, E514S), Patch 6A (pAG 8646; Q806A, L807A, F809A, F810A), and Patch 6B (pAG 8535; D811S, E812S, E814S) were generated using overlap PCR and ligated into pET-15b using NdeI and BamHI. *B. subtilis* MutL N-terminal domain (MutL–NTD) (pAG 8286; residues 1–339) was amplified and ligated into pProEX HTa (Invitrogen) using NcoI and XhoI. All mutants were verified by DNA sequencing (MOBIX, McMaster University).

Purification of his$_6$MutS

Bacillus subtilis MutS variants were overproduced in BL21 (DE3) pRARE or BL21 (DE3) pRARE pLysS cells (Invitrogen) and induced with 1 mM IPTG for 5 h at 25°C. Cells were resuspended in buffer A (20 mM Tris pH 8.0, 0.5 M NaCl, 30 mM imidazole, 1.4 mM 2-mercaptoethanol, and 5% glycerol), lysed by sonication, and clarified by centrifugation at 39 000 *g*. The soluble fraction was purified over a nickel-chelating column equilibrated with buffer A and eluted with 240 mM imidazole. MutS was then injected onto an ion exchange column (Q-Sepharose, GE Healthcare) equilibrated with buffer B (20 mM Tris pH 8.0, 5 mM EDTA, 2.8 mM 2-mercaptoethanol, 100 mM NaCl, and 5% glycerol) and eluted using a linear gradient to 400 mM NaCl. MutS was injected into a gel filtration column (Superdex-200, GE Healthcare) equilibrated with cross-linking buffer (20 mM Hepes pH 7.5, 100 mM NaCl, 5 mM DTT, and 5% glycerol). Protein concentration was measured at 280 nm.

Purification of the MutL N-terminal domain

Bacillus subtilis MutL–NTD was overexpressed in BL21 Star (DE3) cells (Invitrogen) with 0.5 mM IPTG for 5 h at 25°C. MutL–NTD was purified using a nickel chelating column equilibrated with buffer A (pH 9.0) and eluted using 240 mM imidazole. MutL–NTD was then injected into a sizing column (Superdex-200, GE Healthcare) equilibrated with cross-linking buffer. Protein concentration was measured by absorbance at 280 nm.

Spontaneous mutation rate analysis

Fluctuation analysis was performed essentially as described (Bolz *et al*., 2012; Lenhart *et al*., 2013). We inoculated 3 ml of LB with a single colony, and grew at 37°C until an OD_{600} of ~ 1.2. At that point, 1 ml of culture was pelleted and resuspended in 100 μl of saline. A portion of this resuspension was further diluted to 10^{-6}, and plated onto LB plates in order to enumerate the total viable cells with incubation overnight at 30°C to ensure the plates with viable cells did not over grow. The original resuspension was plated on LB supplemented with 150 μg ml^{-1} rifampin plates overnight at 37°C in order to determine the number of spontaneous mutations causing rifampin resistance. After performing a minimum of 15 independent cultures, the mutation rate was determined using the MSS Maximum Likelihood Method using the publicly available FALCOR tool at http://www.mitochondria.org/protocols/FALCOR.html. 95% confidence intervals were determined and percent MMR activity, was determined using the following equation:

[(RMR null – RMR strain)/(RMR null – RMR wild type)]•100 where RMR = relative mutation rate (Hall *et al*., 2009).

Chemical cross-linking

Bacillus subtilis MutS variants (20 μM), 20 μM Mis90, and 20 mM ATP were pre-incubated on ice for 1 h. MutL–NTD (40 μM) was then added with equal volume to the MutS•ATP•DNA reaction and incubated for 30 min at 4°C. Reactions were then incubated with 0.8–1.6 mM bis (sulfosuccinimidyl) suberate (Sigma, BS^3) for 30 min at 22°C. Reactions (10 μl) were quenched with 30 mM Tris pH 7.5 for 15 min at 22°C and separated on a 4–15% SDS gradient gel (Bio-Rad) and stained with Coomassie Blue.

ATPase

ATP hydrolysis assays were performed as previously described (Junop *et al*., 2003) with minor modifications. ATPase activity was measured with 0.3 μM MutS and 5 mM $MgCl_2$ in reaction buffer (20 mM Tris pH 8.0, 90 mM KCl, 1 mM DTT, 1 mg ml^{-1} BSA, and 5% glycerol). Reactions (15 μl) were initiated by the addition of 1 mM α-^{32}P-labelled ATP and incubated for 1 h at 22°C. Reactions were stopped with 25 mM EDTA and hydrolysed product was detected by thin-layer chromatography using 750 mM KH_2PO_4 for running buffer. ATPase activity was measured in triplicates for each MutS variant.

DNA binding

Mis90 is a 90 base pair DNA substrate harbouring a G/T base mismatch (5′ gaaaacctgtatttt**t**cagggcaggcctattggaattcaa catatgaagtcgacgcagctggcggccgcttctagaggatccctcgagaag 3′ annealed to 5′ gcttctcgagggatcctctagaagcggccgccagctgcgtc gacttcatatgttgaattccaataggcctgccctg**g**aaatacaggtttt 3′). MutS (600 pmol) was incubated with equimolar Mis90 in binding buffer (10 mM Hepes pH 7.5, 70 mM KCl, 2 mM DTT, 5 mM $MgCl_2$, 1 mg ml^{-1} BSA, and 15% glycerol) for 1 h on ice. Reactions (15 μl) were resolved on a 6% TBE gel and stained with ethidium bromide. Bands were quantified using ImageJ (http://rsbweb.nih.gov/ij/). DNA binding activity was measured in triplicates for each MutS variant.

Live cell microscopy

Cultures for imaging were prepared as described previously (Dupes *et al*., 2010; Klocko *et al*., 2011; Lenhart *et al*., 2013). Briefly, strains for imaging were inoculated in pre-warmed $S7_{50}$ minimal media supplemented with either 1% L-arabinose or 2% D-glucose at a starting OD_{600} of 0.05. Cells were grown past three doublings to an OD_{600} of 0.4–0.5 and imaged. To treat cultures with the mismatch-forming drug 2-aminopurine, we split the cultures and added a mock treatment to one and 600 μg ml^{-1} 2-aminopurine to the other followed by growth for an additional hour. Cell membranes were visualized with the fluorescent dye TMA-DPH at a working concentration of 10 μM (Lenhart *et al*., 2013). MutS fluorescent fusions were captured with a 1.2 s exposure. Colocalization experiments were conducted with L-arabinose as the sole carbon source, where all other experiments used D-glucose.

In vivo *cross-linking/co-immunoprecipitation*

Bacillus subtilis cultures were inoculated in LB at a starting OD_{600} of 0.05 and grown at 37°C to an OD_{600} of 0.7. Cells were pelleted, washed twice with cross-linking buffer (40 mM HEPES pH 7.4, 500 mM sucrose, 2 mM $MgCl_2$, 150 mM NaCl, 0.02% Tween-20) to remove LB, and resuspended in 1.75 ml of cross-linking buffer. To cross-link intracellular protein complexes, 0.5 mM of DSP was added to the growing cells and cross-linking occurred for 30 min at room temperature on a rotisserrie. Cultures were quenched by adding Tris-HCl (pH 7.5) to a final concentration of 20 mM, and incubated an additional 30 min at room temperature on a rotisserrie. After quenching, cells were lysed via sonication. Lysates were cleared of debris by centrifugation for 30 min at 4°C at 14 000 r.p.m. Lysates were then concentrated to 50 μl, resuspended in cross-linking buffer supplemented with 1× protease inhibitor cocktail and 0.5 mM EDTA to a final volume of 500 μl. A 5% input fraction was pulled from the final volume. The 5% input and the rest of the prepared lysate were incubated overnight on a rotisserie at 4°C. The IP fraction was incubated with 50 μl equilibrated magnetic beads bound with affinity purified α-MutS antisera (MI-1042). In the morning, the lysates were washed 5× for 5 min each with cross-linking buffer on a room temperature rotisserrie. The antibodies were eluted from the magnetic beads by a 10 min incubation in 900 μl of antibody stripping buffer (5 mM

Glycine pH 2.4, 150 mM NaCl). The IP fraction was concentrated by tricarboxylic acid (TCA) precipitation, and resuspended in 1× western loading dye. IP and Input fractions were electrophoresed on the same gel (4–15% gradient gel). Quantitative analysis of the resulting bands was conducted in ImageJ. The numbers represent the statistical mean of 3 independent experiments with the background subtracted from the JSL281 strain. Numbers were determined relative to JSL364 (PY79 wild type strain).

Western and far Western blotting

Bacillus subtilis whole-cell extracts were obtained by centrifuging 25 ml of mid-exponential cultures, followed by resuspension in lysis buffer [10 mM Tris-HCl (pH 7.0), 0.5 mM EDTA, 1 mM AEBSF, 1× Protease Inhibitor cocktail] followed by 3 rounds of sonication (20 Hz, 45 s duration) on ice as described (Lenhart *et al*., 2013). After sonication, SDS was added to a final concentration of 1% and non-soluble cellular debris and whole cells were removed by centrifugation at 4°C. The lysate was divided into one-time use samples and stored at −20°C. Total protein concentration of prepared soluble lysates was determined using Pierce BCA Protein Assay Kit (Thermo Scientific). Equal amounts of total protein were applied to each lane on a 4–15% gradient gel followed by transfer to a nitrocellulose membrane (Simmons and Kaguni, 2003; Simmons *et al*., 2009). Protein levels were determined by using primary antisera: α-MutS (MI-1042), α-MutL (MI-1044), and α-DnaN (MI-1038).

Immunodot blotting was performed as described (Klocko *et al*., 2011). Briefly, equal molar amounts of the indicated proteins were immobilized onto a nitrocellulose membrane with the assistance of a Bio-dot microfiltration apparatus (Bio-Rad). The membrane was incubated in blocking buffer (5% milk solids, 17.4 mM Na_2HPO_4, 2.6 mM NaH_2PO_4, 150 mM NaCl, 0.05% Tween-20, 0.5 mM ATP, 4 mM $MgSO_4$) at 22°C for 1 h. All subsequent washes and incubations took place in blocking buffer. After blocking, the membrane was incubated with 0.4 μM MutL in blocking buffer for 3 h at 22°C. The blot was subsequently washed three times and then incubated in affinity purified α-MutL antisera overnight at 4°C. In the morning, the blot was removed from primary antibody and washed three times at 22°C and placed in secondary antisera (1:2000 α-Rabbit) for 2 h at 22°C. The blot was washed 3 more times, followed by a wash in PBS (17.4 mM Na_2HPO_4, 2.6 mM NaH_2PO_4, 150 mM NaCl, 0.05% Tween-20) to remove excess milk solids and exposed.

Acknowledgements

We thank members of the Simmons and Guarné laboratories for helpful discussions and comments on this manuscript. We would also like to thank Nicholas Bolz for assistance in early cloning and mutagenesis assays. This work was supported by grant MCB1050948 from the National Science Foundation to L.A.S. and by a Discovery Grant from the Natural Sciences and Engineering Research Council of Canada (NSERC) to A.G. In addition, M.C.P. was supported in part by a doctoral scholarship from NSERC and J.S.L. was supported in part by a predoctoral fellowship from the Rackham Graduate School at the University of Michigan.

References

Acharya, S., Foster, P.L., Brooks, P., and Fishel, R. (2003) The coordinated functions of the *E. coli* MutS and MutL proteins in mismatch repair. *Mol Cell* **12:** 233–246.

Arnold, K., Bordoli, L., Kopp, J., and Schwede, T. (2006) The SWISS-MODEL workspace: a web-based environment for protein structure homology modelling. *Bioinformatics* **22:** 195–201.

Ban, C., and Yang, W. (1998) Crystal structure and ATPase activity of MutL: implications for DNA repair and mutagenesis. *Cell* **95:** 541–552.

Ban, C., Junop, M., and Yang, W. (1999) Transformation of MutL by ATP binding and hydrolysis: a switch in DNA mismatch repair. *Cell* **97:** 85–97.

Berkmen, M.B., and Grossman, A.D. (2006) Spatial and temporal organization of the *Bacillus subtilis* replication cycle. *Mol Microbiol* **62:** 57–71.

Bjornson, K.P., Allen, D.J., and Modrich, P. (2000) Modulation of MutS ATP hydrolysis by DNA cofactors. *Biochemistry* **39:** 3176–3183.

Blackwell, L.J., Bjornson, K.P., Allen, D.J., and Modrich, P. (2001) Distinct MutS DNA-binding modes that are differentially modulated by ATP binding and hydrolysis. *J Biol Chem* **276:** 34339–34347.

Bolz, N.J., Lenhart, J.S., Weindorf, S.C., and Simmons, L.A. (2012) Residues in the N-terminal domain of MutL required for mismatch repair in *Bacillus subtilis*. *J Bacteriol* **194:** 5361–5367.

Cooper, L.A., Simmons, L.A., and Mobley, H.L. (2012) Involvement of mismatch repair in the reciprocal control of motility and adherence of uropathogenic *Escherichia coli*. *Infect Immun* **80:** 1969–1979.

Cox, E.C., Degnen, G.E., and Scheppe, M.L. (1972) Mutator gene studies in *Escherichia coli*: the *mutS* gene. *Genetics* **72:** 551–567.

Dalrymple, B.P., Kongsuwan, K., Wijffels, G., Dixon, N.E., and Jennings, P.A. (2001) A universal protein-protein interaction motif in the eubacterial DNA replication and repair systems. *Proc Natl Acad Sci USA* **98:** 11627–11632.

Davies, B.W., Bogard, R.W., Dupes, N.M., Gerstenfeld, T.A., Simmons, L.A., and Mekalanos, J.J. (2011) DNA damage and reactive nitrogen species are barriers to *Vibrio cholerae* colonization of the infant mouse intestine. *PLoS Pathog* **7:** e1001295.

Dherin, C., Gueneau, E., Francin, M., Nunez, M., Miron, S., Liberti, S.E., *et al.* (2009) Characterization of a highly conserved binding site of Mlh1 required for exonuclease I-dependent mismatch repair. *Mol Cell Biol* **29:** 907–918.

Dupes, N.M., Walsh, B.W., Klocko, A.D., Lenhart, J.S., Peterson, H.L., Gessert, D.A., *et al.* (2010) Mutations in the *Bacillus subtilis* beta clamp that separate its roles in DNA replication from mismatch repair. *J Bacteriol* **192:** 3452–3463.

Fishel, R., Lescoe, M.K., Rao, M.R.S., Copeland, N.G., Jenkins, N.A., Garber, J., *et al.* (1993) The human mutator gene homolog *MSH2* and its association with hereditary nonpolyposis cancer. *Cell* **75:** 1027–1038.

Fishel, R., Ewel, A., Lee, S., Lescoe, M.K., and Griffith, J. (1994) Binding of mismatched microsatellite DNA sequences by the human MSH2 protein. *Science* **266:** 1403–1405.

Ginetti, F., Perego, M., Albertini, A.M., and Galizzi, A. (1996) *Bacillus subtilis mutS mutL* operon: identification, nucleotide sequence and mutagenesis. *Microbiology* **142** (Part 8): 2021–2029.

Gorman, J., Wang, F., Redding, S., Plys, A.J., Fazio, T., Wind, S., *et al*. (2012) Single-molecule imaging reveals target-search mechanisms during DNA mismatch repair. *Proc Natl Acad Sci USA* **109:** E3074–E3083.

Gradia, S., Subramanian, D., Wilson, T., Acharya, S., Makhov, A., Griffith, J., and Fishel, R. (1999) hMSH2-hMSH6 forms a hydrolysis-independent sliding clamp on mismatched DNA. *Mol Cell* **3:** 255–261.

Guarne, A., Ramon-Maiques, S., Wolff, E.M., Ghirlando, R., Hu, X., Miller, J.H., and Yang, W. (2004) Structure of the MutL C-terminal domain: a model of intact MutL and its roles in mismatch repair. *EMBO J* **23:** 4134–4145.

Habraken, Y., Sung, P., Prakash, L., and Prakash, S. (1997) Enhancement of MSH2-MSH3-mediated mismatch recognition by the yeast MLH1-PMS1 complex. *Curr Biol* **7:** 790–793.

Hall, B.M., Ma, C.X., Liang, P., and Singh, K.K. (2009) Fluctuation analysis CalculatOR: a web tool for the determination of mutation rate using Luria-Delbruck fluctuation analysis. *Bioinformatics* **25:** 1564–1565.

Hamilton, S.R., Liu, B., Parsons, R.E., Papadopoulos, N., Jen, J., Powell, S.M., *et al*. (1995) The molecular basis of Turcot's syndrome. *N Engl J Med* **332:** 839–847.

Hombauer, H., Campbell, C.S., Smith, C.E., Desai, A., and Kolodner, R.D. (2011) Visualization of eukaryotic DNA mismatch repair reveals distinct recognition and repair intermediates. *Cell* **147:** 1040–1053.

Iyer, R.R., Pluciennik, A., Burdett, V., and Modrich, P.L. (2006) DNA mismatch repair: functions and mechanisms. *Chem Rev* **106:** 302–323.

Iyer, R.R., Pluciennik, A., Genschel, J., Tsai, M.S., Beese, L.S., and Modrich, P. (2010) MutLalpha and proliferating cell nuclear antigen share binding sites on MutSbeta. *J Biol Chem* **285:** 11730–11739.

Junop, M.S., Yang, W., Funchain, P., Clendenin, W., and Miller, J.H. (2003) *In vitro* and *in vivo* studies of MutS, MutL and MutH mutants: correlation of mismatch repair and DNA recombination. *DNA Repair (Amst)* **2:** 387–405.

Kijas, A.W., Studamire, B., and Alani, E. (2003) Msh2 separation of function mutations confer defects in the initiation steps of mismatch repair. *J Mol Biol* **331:** 123–138.

Klein, E., Smith, D.L., and Laxminarayan, R. (2007) Hospitalizations and deaths caused by methicillin-resistant *Staphylococcus aureus*, United States, 1999-2005. *Emerg Infect Dis* **13:** 1840–1846.

Klevens, R.M., Morrison, M.A., Nadle, J., Petit, S., Gershman, K., Ray, S., *et al*. (2007) Invasive methicillin-resistant *Staphylococcus aureus* infections in the United States. *JAMA* **298:** 1763–1771.

Klocko, A.D., Crafton, K.M., Walsh, B.W., Lenhart, J.S., and Simmons, L.A. (2010) Imaging mismatch repair and cellular responses to DNA damage in *Bacillus subtilis*. *J Vis Exp* **36:** 1–4.

Klocko, A.D., Schroeder, J.W., Walsh, B.W., Lenhart, J.S., Evans, M.L., and Simmons, L.A. (2011) Mismatch repair causes the dynamic release of an essential DNA polymerase from the replication fork. *Mol Microbiol* **82:** 648–663.

Kluytmans, J., van Belkum, A., and Verbrugh, H. (1997) Nasal carriage of *Staphylococcus aureus*: epidemiology, underlying mechanisms, and associated risks. *Clin Microbiol Rev* **10:** 505–520.

Kunkel, T.A., and Erie, D.A. (2005) DNA mismatch repair. *Annu Rev Biochem* **74:** 681–710.

Lamers, M.H., Perrakis, A., Enzlin, J.H., Winterwerp, H.H., de Wind, N., and Sixma, T.K. (2000) The crystal structure of DNA mismatch repair protein MutS binding to a G x T mismatch. *Nature* **407:** 711–717.

Landgraf, D., Okumus, B., Chien, P., Baker, T.A., and Paulsson, J. (2012) Segregation of molecules at cell division reveals native protein localization. *Nat Methods* **9:** 480–482.

Larrea, A.A., Lujan, S.A., and Kunkel, T.A. (2010) SnapShot: DNA mismatch repair. *Cell* **141:** 730 e731.

Lemon, K.P., and Grossman, A.D. (1998) Localization of bacterial DNA polymerase: evidence for a factory model of replication. *Science* **282:** 1516–1519.

Lemon, K.P., and Grossman, A.D. (2000) Movement of replicating DNA through a stationary replisome. *Mol Cell* **6:** 1321–1330.

Lenhart, J.S., Schroeder, J.W., Walsh, B.W., and Simmons, L.A. (2012) DNA repair and genome maintenance in *Bacillus subtilis*. *Microbiol Mol Biol Rev* **76:** 530–564.

Lenhart, J.S., Sharma, A., Hingorani, M.M., and Simmons, L.A. (2013) DnaN clamp zones provide a platform for spatiotemporal coupling of mismatch detection to DNA replication. *Mol Microbiol* **87:** 553–568.

Lowy, F.D. (1998) *Staphylococcus aureus* infections. *N Engl J Med* **339:** 520–532.

Mendillo, M.L., Hargreaves, V.V., Jamison, J.W., Mo, A.O., Li, S., Putnam, C.D., *et al*. (2009) A conserved MutS homolog connector domain interface interacts with MutL homologs. *Proc Natl Acad Sci USA* **106:** 22223–22228.

Nystrom-Lahti, M., Perrera, C., Raschle, M., Panyushkina-Seiler, E., Marra, G., Curci, A., *et al*. (2002) Functional analysis of MLH1 mutations linked to hereditary nonpolyposis colon cancer. *Genes Chromosomes Cancer* **33:** 160–167.

Obmolova, G., Ban, C., Hsieh, P., and Yang, W. (2000) Crystal structures of mismatch repair protein MutS and its complex with a substrate DNA. *Nature* **407:** 703–710.

Peltomaki, P. (2005) Lynch syndrome genes. *Fam Cancer* **4:** 227–232.

Pillon, M.C., Lorenowicz, J.J., Uckelmann, M., Klocko, A.D., Mitchell, R.R., Chung, Y.S., *et al*. (2010) Structure of the endonuclease domain of MutL: unlicensed to cut. *Mol Cell* **39:** 145–151.

Plotz, G., Welsch, C., Giron-Monzon, L., Friedhoff, P., Albrecht, M., Piiper, A., *et al*. (2006) Mutations in the MutSalpha interaction interface of MLH1 can abolish DNA mismatch repair. *Nucleic Acids Res* **34:** 6574–6586.

Prolla, T.A., Pang, Q., Alani, E., Kolodner, R.D., and Liskay, R.M. (1994) MLH1, PMS1, and MSH2 interactions during the initiation of DNA mismatch repair in yeast. *Science* **265:** 1091–1093.

Prudhomme, M., Martin, B., Mejean, V., and Claverys, J.P. (1989) Nucleotide sequence of the *Streptococcus pneumoniae hexB* mismatch repair gene: homology of *HexB* to

MutL of *Salmonella typhimurium* and to *PMS1* of *Saccharomyces cerevisiae*. *J Bacteriol* **171:** 5332–5338.
Sacho, E.J., Kadyrov, F.A., Modrich, P., Kunkel, T.A., and Erie, D.A. (2008) Direct visualization of asymmetric adenine-nucleotide-induced conformational changes in MutL alpha. *Mol Cell* **29:** 112–121.
Schofield, M.J., and Hsieh, P. (2003) DNA mismatch repair: molecular mechanisms and biological function. *Annu Rev Microbiol* **57:** 579–608.
Simmons, L.A., and Kaguni, J.M. (2003) The DnaAcos allele of *Escherichia coli*: hyperactive initiation is caused by substitution of A184V and Y271H, resulting in defective ATP binding and aberrant DNA replication control. *Mol Microbiol* **47:** 755–765.
Simmons, L.A., Davies, B.W., Grossman, A.D., and Walker, G.C. (2008) Beta clamp directs localization of mismatch repair in *Bacillus subtilis*. *Mol Cell* **29:** 291–301.
Simmons, L.A., Goranov, A.I., Kobayashi, H., Davies, B.W., Yuan, D.S., Grossman, A.D., and Walker, G.C. (2009) Comparison of responses to double-strand breaks between *Escherichia coli* and *Bacillus subtilis* reveals different requirements for SOS induction. *J Bacteriol* **191:** 1152–1161.
Smith, B.T., Grossman, A.D., and Walker, G.C. (2001) Visualization of mismatch repair in bacterial cells. *Mol Cell* **8:** 1197–1206.
Umar, A., Boyer, J.C., Thomas, D.C., Nguyen, D.C., Risinger, J.I., Boyd, J., *et al*. (1994) Defective mismatch repair in extracts of colorectal and endometrial cancer cell lines exhibiting microsatellite instability. *J Biol Chem* **269:** 14367–14370.
Winkler, I., Marx, A.D., Lariviere, D., Heinze, R.J., Cristovao, M., Reumer, A., *et al*. (2011) Chemical trapping of the dynamic MutS-MutL complex formed in DNA mismatch repair in *Escherichia coli*. *J Biol Chem* **286:** 17326–17337.
Wojtaszek, J., Lee, C.J., D'Souza, S., Minesinger, B., Kim, H., D'Andrea, A.D., *et al*. (2012a) Structural basis of Rev1-mediated assembly of a quaternary vertebrate translesion polymerase complex consisting of Rev1, heterodimeric polymerase (Pol) zeta, and Pol kappa. *J Biol Chem* **287:** 33836–33846.
Wojtaszek, J., Liu, J., D'Souza, S., Wang, S., Xue, Y., Walker, G.C., and Zhou, P. (2012b) Multifaceted recognition of vertebrate Rev1 by translesion polymerases zeta and kappa. *J Biol Chem* **287:** 26400–26408.

Supporting information

Additional supporting information may be found in the online version of this article at the publisher's web-site.